

Supplementary Information: Particle shape tunes fragility in hard polyhedron glass-formers

Erin G. Teich,¹ Greg van Anders,^{1,2,3} and Sharon C. Glotzer^{1,2,3,4}

¹*Applied Physics Program, University of Michigan, Ann Arbor MI 48109^a*

²*Department of Physics, University of Michigan, Ann Arbor MI 48109*

³*Department of Chemical Engineering, University of Michigan, Ann Arbor MI 48109^b*

⁴*Biointerfaces Institute, University of Michigan, Ann Arbor MI 48109*

(Dated: 25 August 2020)

S1. STATIC STRUCTURE FACTORS

Static structure factors for all systems studied in this paper are shown in Fig. S1 and were calculated for the first frame of each trajectory following equilibration. Detail regarding the calculation can be found in the *Supplementary Information* of Ref. 1. Systems at $(\alpha_a, \alpha_c) = (0, 0.5)$, $(0, 0.6)$, and $(0, 0.7)$ display a so-called “pre-peak,” or “first sharp diffraction peak,” which indicates intermediate-range ordering commonly seen in network glass-formers²⁻⁴.

S2. KWW FITS

As described in the main text, we determined relaxation times for all systems by the average of all values $\{t\}$ for which $|\text{Re } F_s(k, t) - \text{Re } F_s(k, 0)/e| < \Delta$, where Δ is a tolerance chosen from the set $\{0.01, 0.05, 0.1\}$ to give a relaxation time τ_α that produced the best fit of $\text{Re } F_s(k, t)$ to a Kohlrausch-Williams-Watts (KWW)^{5,6} stretched exponential functional form, $B \exp[-(t/\tau_\alpha)^\beta]$, at all densities. We varied B and β as fitting parameters. We fit the final fraction f of $\text{Re } F_s(k, t)$ at all densities, and chose f from the set $\{0.99, 0.95, 0.9, 0.8, 0.7\}$ such that it produced the best fit. We only considered data for which $\text{Re } F_s(k, t) > 0.01$ to avoid unnecessary fitting to long tails at zero.

Fig. S2 shows the real self-part of the intermediate scattering function $F_s(k, t)$ rescaled by relaxation time for all systems, as well as the best KWW fit. We observe that the systems each generally obey a so-called “time-temperature superposition”⁷ during late α -relaxation, indicated by the collapse of the curves.

S3. PRESSURE RATHER THAN DENSITY AS A CONTROL PARAMETER

As described in the main text, compelling arguments exist⁸ for the use of reduced pressure as the relevant control parameter in hard particle systems, rather than density. Here, we show an analysis of the relaxation behavior of our systems over reduced pressure rather than density. Curiously, because of these systems’ very different dependencies of $Z \equiv \beta p/\rho$ on ϕ (Fig. S3D), behavior in these systems at $Z < Z_C$ seems to show that, at lower pressures, the less tetrahedral particle shape (in pink) appears strong with pressure used as the control parameter, while the more tetrahedral particle shapes (the redder curves) are more fragile with pressure used as the control parameter (Figs. S3A and S3B). When $Z > Z_C$, however, the relaxation times τ_α still fall off of the best VFT fit to the data at lower pressure. This drop in relaxation time means that the numerical derivative of these data points with respect to Z/Z_C , $s(Z/Z_C) \equiv \partial \log \tau_\alpha / \partial (Z/Z_C)$, also drops at high pressure (Fig. S3C). At the highest pressures, $s(Z/Z_C)$ for two of the three more tetrahedral particle shapes (the redder curves) drops below $s(Z/Z_C)$ for the least tetrahedral particle shape (in pink), and the remaining more tetrahedral particle shape also shows a downward trend in $s(Z/Z_C)$. As discussed in the main text, the drop in this slope indicates that at high pressure, these systems are less fragile. Thus, our general finding, that more tetrahedral particles are less fragile on approach to the glass transition, holds even when using reduced pressure as a control parameter instead of density.

S4. FWHM OF BOND ANGLE DISTRIBUTIONS

Full widths at half maximum (FWHM) of bond angle distributions are plotted in Fig. S4 for $(\alpha_a, \alpha_c) = (0, 0.5)$, $(0, 0.6)$, and $(0, 0.7)$, at all measured values of ϕ . As ϕ increases, FWHM decreases. At almost all values of ϕ , more tetrahedral particle shapes have lower FWHM values.

^aNow at Department of Bioengineering, University of Pennsylvania, Philadelphia PA 19104

^bNow at Department of Physics, Engineering Physics & Astronomy, Queen’s University, Kingston ON K7L 3N6

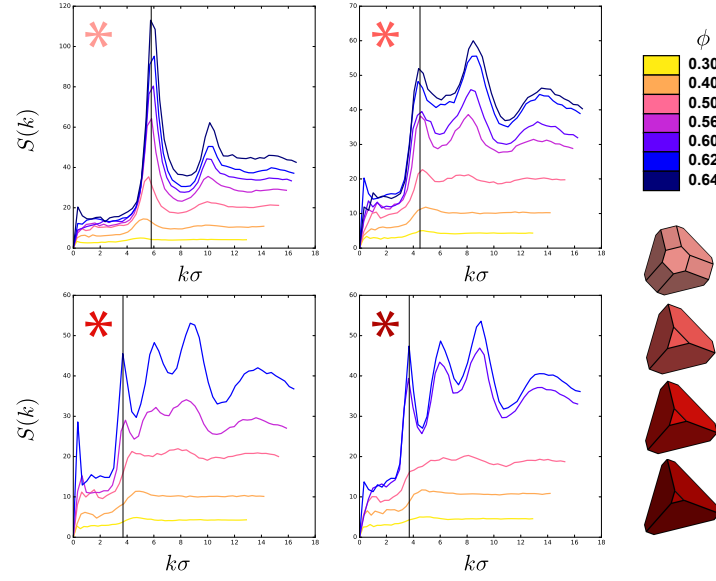


FIG. S1: Static structure factors for all systems. Static structure factors are given as functions of $k\sigma$, where σ is a length scale that characterizes the particle size of each system: $\sigma^3 = v_p$, where v_p is the particle volume. Vertical lines through each plot indicate the position of the first peak, used for calculation of the self-intermediate scattering function. These positions are $k\sigma = 5.8, 4.5, 3.7, 3.7$ for $(\alpha_a, \alpha_c) = (0.2, 0.5), (0, 0.5), (0, 0.6),$ and $(0, 0.7)$, respectively.

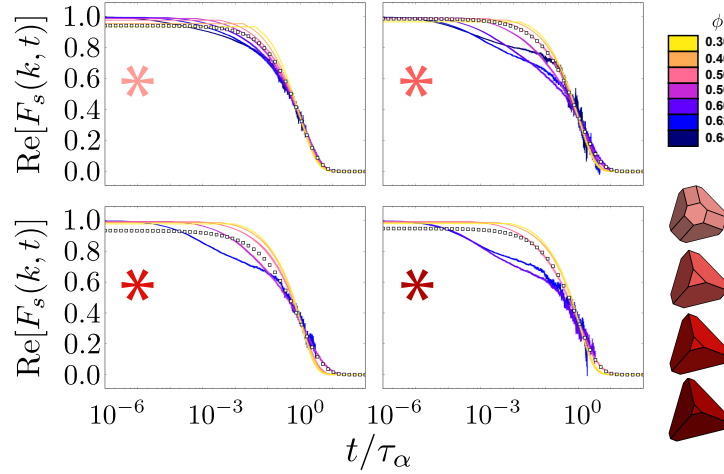


FIG. S2: The real part of the self-intermediate scattering function as a function of rescaled time, for indicated state points. The optimal KWW fit is shown in white squares.

TABLE S1: Parameters associated with VFT fits of relaxation time in our systems. τ_∞ is in units of 10 MC sweeps.

α_a	α_c	ϕ_0	τ_∞	A	ϕ_C
0.2	0.5	0.800	9.760	0.284	0.631
0.0	0.5	0.762	42.460	0.183	0.615
0.0	0.6	0.812	32.220	0.356	0.610
0.0	0.7	0.811	26.056	0.416	0.596

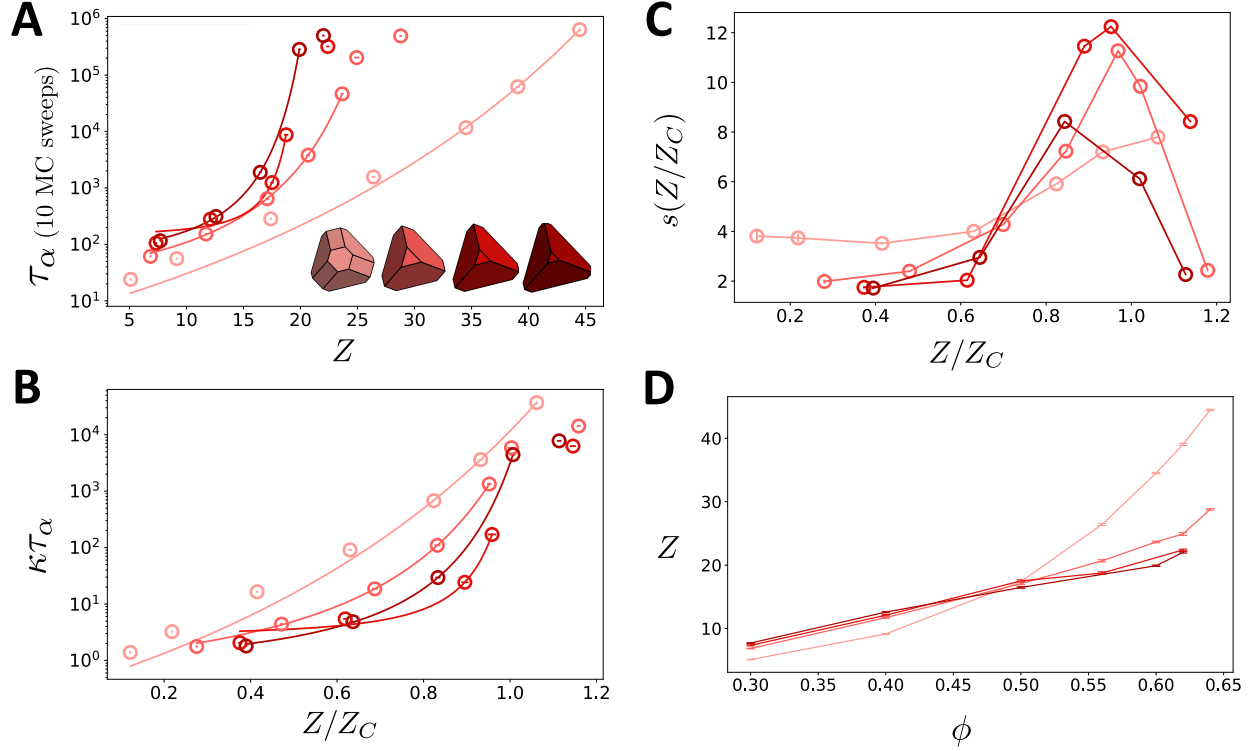


FIG. S3: Glass-forming systems exhibit a range of fragilities, with systems generally becoming “stronger” at high pressure as particle shapes become increasingly tetrahedral, indicated by increasingly red color. (A) An Angell plot of relaxation time as a function of reduced pressure $Z \equiv \beta p/\rho$. Relaxation time is in units of 10 MC sweeps. Solid lines through the data points are VFT fits to relaxation time, given by $\tau_{\alpha}^{VFT}(Z) = \tau_{\infty} \exp\left[\frac{A}{(Z_0 - Z)^2}\right]$. They pass only through the data points that were actually fit. Error bars for each relaxation time are smaller than the marker size, and described in the main text. (B) A scaled Angell plot, where pressure is scaled by Z_C (defined for each system by $\tau_{\alpha}^{VFT}(Z_C) = 2$ million MC sweeps) and relaxation time is scaled by κ (defined for each system by $\kappa^{-1} = \tau_{\alpha}^{MCT}(Z = 3)$). The mode-coupling theory (MCT) fit at low pressures is given by $\tau_{\alpha}^{MCT}(Z) = A(Z_0 - Z)^{-\gamma}$, and not shown. Error bars are scaled appropriately and remain smaller than the marker size. (C) Numerical slope of the log of relaxation time as a function of scaled pressure, $s(Z/Z_C) \equiv \partial \log \tau_{\alpha} / \partial (Z/Z_C)$, showing that more tetrahedral particle shapes have stronger behavior at the highest pressures investigated. Error bars are smaller than the marker size, and described in the main text. (D) Equations of state of all systems, showing very different dependencies of reduced pressure $Z \equiv \beta p/\rho$ on volume fraction ϕ . At each density, pressure was calculated every 10 million MC sweeps using a volume perturbation technique^{9–11} that extrapolates pressure in hard particle isochoric simulations through evaluations of the volume scaling needed to cause particle-pair overlaps throughout the system.

Its implementation in HOOMD-blue is detailed elsewhere^{12,13}. Data points are means of 10 pressure values calculated over each system trajectory, and error bars are the standard error of the mean.

S5. BOND ANGLES FOR $(\alpha_a, \alpha_c) = (0.2, 0.5)$

Fig. S5 shows bond angle distributions for the system at $(\alpha_a, \alpha_c) = (0.2, 0.5)$ for densities $\phi = [0.3, 0.4, 0.5, 0.56, 0.6, 0.62, 0.64]$, plotted in colors ranging from light gray (for $\phi = 0.3$) to dark gray (for $\phi = 0.64$). Bond angle distributions were calculated using methods described in the main text. The distributions become increasingly bimodal with increasing density: the peak at $\sim 116.6^\circ$ remains consistent with increasing density, while a second peak moves from $\sim 63.4^\circ$ at $\phi = 0.3$ to $\sim 70.9^\circ$ at $\phi =$

0.64. Dotted lines demarcate these peaks. Distributions of bond angle were also calculated for three relevant crystal structures: *bcc* (shown in blue), γ -brass (shown in purple) and *fcc* (shown in green). Several of these peaks, particularly for *bcc* and γ -brass, are near the peaks of the bimodal $(\alpha_a, \alpha_c) = (0.2, 0.5)$ distributions. *bcc*, *fcc*, and γ -brass are structures that crystallize in regions of shape space that lie close to the glass-former at $(\alpha_a, \alpha_c) = (0.2, 0.5)$, as noted in the main text. We found bond angles for these crystals in all cases by constructing the crystals manually, then employing identical methods to those

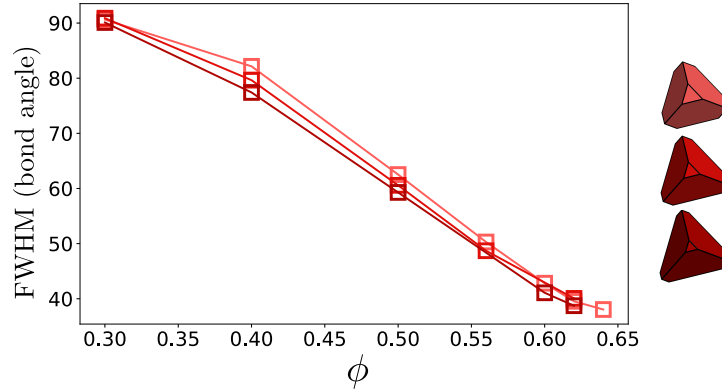


FIG. S4: Full widths at half maximum (FWHM) of bond angle distributions at a variety of densities ϕ and particle shapes. Particles are drawn to the right of the plot. Colors of the FWHM markers and connecting lines identify the particle shape of each system. As ϕ increases, FWHM decreases. At almost all values of ϕ , more tetrahedral particle shapes (with smaller vertex truncation) have lower FWHM values.

used for the glass-forming system to find bond angles between each particle in the crystal and all possible two-neighbor subsets of its four nearest neighbors. Since the crystals have different numbers of particles in their unit cells, bond-angle distributions are shown as the fraction of all calculated bond-angles with values in ranges indicated by the discrete bars. Scales for these plots are located on the right axis of Fig. S5; 0 values are omitted in the interest of space, but located at the x-axis of each plot.

It should be noted that the bond-angles at $\sim 63.4^\circ$ and $\sim 116.6^\circ$ are in fact the angles associated with a local icosahedral environment: each is an angle between a pair of vectors pointing from the center of an icosahedron to two of its vertices. Exactly, they are (in radians) $\pi/2 \pm \arctan(1/2)$. Icosahedral local structure is well-known to be prevalent in supercooled metallic systems^{14–16} or other simple liquids^{17–19}. γ -brass also contains bond-angles close to the icosahedral angles because it contains closely-packed local environments. Thus, the system at $(\alpha_a, \alpha_c) = (0.2, 0.5)$ seems to shift with density from local environments characterized by icosahedral (and γ -brass-like) angles to local environments characterized by icosahedral angles and *bcc*-like angles. This may be a further indication of structural competition, as explored in Ref. 1. The curious migration of the first bond angle peak from an icosahedral angle to a *bcc*-like angle is a phenomenon for future study.

¹E. G. Teich, G. van Anders, and S. C. Glotzer, “Identity crisis in alchemical space drives the entropic colloidal glass transition,” *Nature Communications* **10**, 64 (2019).

²S. R. Elliott, “Medium-range structural order in covalent amorphous solids,” *Nature* **354**, 445–452 (1991).

³S. R. Elliott, “Origin of the first sharp diffraction peak in

the structure factor of covalent glasses,” *Physical Review Letters* **67**, 711–714 (1991), arXiv:0000135489.

⁴I. Saika-Voivod, F. Smallenburg, and F. Sciortino, “Understanding tetrahedral liquids through patchy colloids,” *Journal of Chemical Physics* **139** (2013), 10.1063/1.4840695, arXiv:1309.2198.

⁵R. Kohlrausch, “Theorie des elektrischen Rückstandes in der Leidener Flasche,” *Annalen der Physik und Chemie* **167**, 179–214 (1854).

⁶G. Williams and D. C. Watts, “Non-symmetrical dielectric relaxation behaviour arising from a simple empirical decay function,” *Transactions of the Faraday Society* **66**, 80 (1970), arXiv:0001055v2 [arXiv:cond-mat].

⁷L. Berthier and G. Biroli, “Theoretical perspective on the glass transition and amorphous materials,” *Reviews of Modern Physics* **83**, 587–645 (2011), arXiv:1011.2578.

⁸L. Berthier and T. a. Witten, “Glass transition of dense fluids of hard and compressible spheres,” *Physical Review E* **80**, 021502 (2009).

⁹R. Eppenga and D. Frenkel, “Monte carlo study of the isotropic and nematic phases of infinitely thin hard platelets,” *Molecular Physics* **52**, 1304–1334 (1984).

¹⁰M. P. Allen, “Evaluation of pressure tensor in constant-volume simulations of hard and soft convex bodies,” *Journal of Chemical Physics* **124** (2006), 10.1063/1.2202352, arXiv:0603027 [cond-mat].

¹¹P. E. Brumby, A. J. Haslam, E. De Miguel, and G. Jackson, “Subtleties in the calculation of the pressure and pressure tensor of anisotropic particles from volume-perturbation methods and the apparent asymmetry of the compressive and expansive contributions,” *Molecular Physics* **109**, 169–189 (2011).

¹²J. A. Anderson, E. Jankowski, T. L. Grubb, M. Engel, and S. C. Glotzer, “Massively parallel monte carlo for many-particle simulations on GPUs,” *Journal of Computational Physics* **254**, 27–38 (2013), arXiv:1211.1646v2.

¹³J. A. Anderson, M. Eric Irrgang, and S. C. Glotzer, “Scalable Metropolis Monte Carlo for simulation of hard shapes,” *Computer Physics Communications* **204**, 21–30 (2015).

¹⁴T. Schenk, D. Holland-Moritz, V. Simonet, R. Bellissent, and D. M. Herlach, “Icosahedral Short-Range Order in Deeply Undercooled Metallic Melts,” *Physical Review Letters* **89**, 075507 (2002).

¹⁵K. F. Kelton, G. W. Lee, A. K. Gangopadhyay, R. W. Hy-

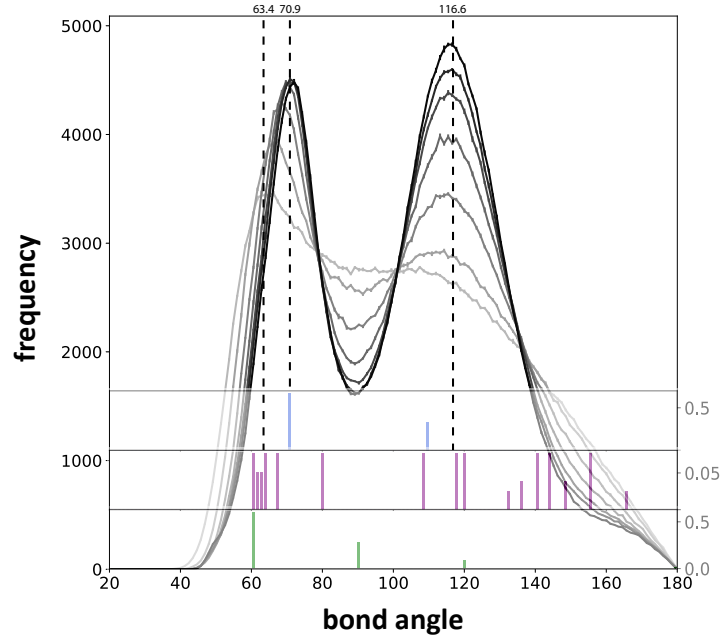


FIG. S5: Bond angle distributions for the system at $(\alpha_a, \alpha_c) = (0.2, 0.5)$ for densities $\phi = [0.3, 0.4, 0.5, 0.56, 0.6, 0.62, 0.64]$, plotted in colors ranging from light gray (for $\phi = 0.3$) to dark gray (for $\phi = 0.64$).

Dotted lines show peak locations and their values are written at the top of the plot. Crystal bond-angle distributions, calculated as fractions of bond-angles in the unit cell with value ranges shown by the bars, are plotted for *bcc* (blue), γ -brass (purple), and *fcc* (green) crystal structures. Their scales are on the right axis of the plot.

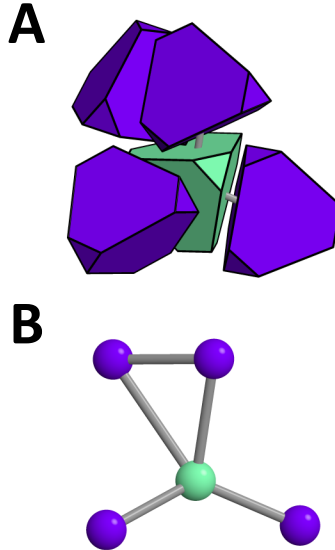


FIG. S6: (A) An example snapshot of a bond-angle of approximately 45° in a system at $(\alpha_a, \alpha_c) = (0, 0.5)$. The acute angle is between the green particle in the center and its two nearest neighbors, face-to-face with each other, at the top of the snapshot. (B) Centers of mass of all particles, with bonds drawn between them to guide the eye.

- ers, T. J. Rathz, J. R. Rogers, M. B. Robinson, and D. S. Robinson, "First X-Ray Scattering Studies on Electrostatically Levitated Metallic Liquids: Demonstrated Influence of Local Icosahedral Order on the Nucleation Barrier," *Physical Review Letters* **90**, 195504 (2003).
- ¹⁶Y. Q. Cheng and E. Ma, "Atomic-level structure and structure – property relationship in metallic glasses," *Progress in Materials Science* **56**, 379–473 (2011).
- ¹⁷F. C. Frank, "Supercooling of Liquids," *Proceedings of the Royal Society A: Mathematical, Physical and Engineering Sciences* **215**, 43–46 (1952).
- ¹⁸H. Jónsson and H. C. Andersen, "Icosahedral Ordering in the Lennard-Jones Liquid and Glass," *Physical Review Letters* **60**, 2295–2298 (1988).
- ¹⁹M. Leocmach and H. Tanaka, "Roles of icosahedral and crystal-like order in the hard spheres glass transition," *Nature Communications* **3**, 974 (2012).